Star-shaped fluorene-BODIPY oligomers: versatile donor-acceptor systems for luminescent solar concentrators

Nathaniel J. L. K. Davis, Rowan W. MacQueen, Saul T. E. Jones, Clara Orofino-Pena, Diego Cortizo-Lacalle, Rupert G. D. Taylor, Dan Credgington, Peter J. Skabara and Neil C. Greenham

Contacts

Nathaniel J. L. K. Davis, Saul T. E. Jones, Dan Credgington and Prof. Neil C. Greenham*

Cavendish Laboratory, University of Cambridge, J.J. Thomson Avenue, Cambridge, CB3 0HE, UK, Email: ncg11@cam.ac.uk

Dr Clara Orofino, Dr Diego Cortizo-Lacalle, Dr Rupert G. D. Taylor and Prof. Peter J. Skabara

WestCHEM, Department of Pure and Applied Chemistry, University of Strathclyde, 295 Cathedral St, Glasgow G1 1XL, UK

Dr Rowan W. MacQueen

Institute for Nanospectroscopy, Helmholtz-Zentrum Berlin für Materialien und Energie GmbH, Albert-Einstein-Str. 15, 12489 Berlin, Germany

Abstract

Luminescent solar concentrators (LSCs) are waveguides doped with luminescent centers that can spectrally and spatially concentrate sunlight. They can reduce the cost of photovoltaic energy production and are attractive prospects for photobioreactors and building-integrated applications. Reabsorption, caused by non-zero overlap between the absorption and emission spectra of the light-emitting centers, often limits LSC efficiency. Donor-acceptor energy-transfer complexes are one method to mitigate reabsorption by shifting the emission away from the main absorption peak. Here we introduce versatile star-shaped donor-acceptor molecules based on a central BODIPY energy acceptor with oligofluorene donor side units. Varying the oligofluorene chain length alters the relative oscillator strengths of the donor and acceptor, changing the severity of reabsorption for a given donor density, but also changing the luminescence yield and emission spectrum. We performed comprehensive device measurements and Monte Carlo ray tracing simulations of LSCs containing three oligofluorene-BODIPY donor-acceptor systems with different oligofluorene chain lengths, and then extended the simulation to study hypothetical analogs with higher donor-acceptor ratios and different terminal acceptors. We found that the measured structures permit waveguide propagation lengths on a par with state-of-the-art nanocrystalline emitters, while the proposed structures are viable candidates for photobioreactor and energy production roles and should be synthesized.

Introduction

Luminescent solar concentrators (LSCs) consist of a transparent waveguide doped with highly luminescent chromophores. Sunlight incident on the LSC is absorbed by the chromophores and emitted into waveguide modes, confining the light for transport to a useful output[1]. As the input aperture of an LSC is larger than the output aperture, LSCs can concentrate light spatially as well as spectrally (Figure 1 (a)). Photovoltaic (PV) cells can be attached to the output aperture, increasing the photon flux available to the cell compared to direct illumination by sunlight[2–4]. The narrow emission spectrum of the LSC can also be tuned to improve conversion efficiency[4]. The primary motivation for this LSC-PV combination has traditionally been the high cost of PV cells, with the LSCs intended as a cheap replacement for large areas of expensive cell. However, as the cost of PV modules has decreased, other applications are under consideration. The aesthetic and structural properties of LSCs are being viewed as increasingly important[1]. PV modules in general are heavy, non-structural, and available in limited colors, while LSCs are light, can be formed into a range of shapes and as part of structures, and are colorful. This makes them a strong prospect for integration into energy-generating structures[2,4]. In addition, LSCs are being explored as a means to enhance photobioreactors[5], as daylighting sources[6] and as antennae for visible-light communications[7].

The power conversion efficiency (PCE) of an LSC is given by $PCE \approx \eta_{abs}\eta_{stokes}\eta_{em}\eta_{prop}(G)$, where η_{abs} is the absorbed fraction of the solar spectrum, η_{stokes} is the fraction of energy lost in down conversion, η_{em} is the probability of remission into waveguide modes, and η_{prop} accounts for all the propagation-related losses. *G*, the geometric ratio, is the ratio of input to output aperture areas[8–10]. The need to guide light over long distances within a heavily-doped matrix means reabsorption typically dominates the losses embedded in η_{prop}[4,11,12], except in unusual cases of emitters with very large Stokes shifts where parasitic matrix losses take over[13].

Reabsorption can be diminished by increasing the Stokes shift of the emitting chromophore[14], or through separating the absorbing and emitting chromophores and minimizing the concentration of the latter[15–17]. Increasing Stokes shift directly is typically pursued for inorganic emitters such as quantum dots, where varying composition and size, and the use of core-shell structures, allow the absorption and emission properties to be controlled[18,19]. For organic molecules where the Stokes shift may be considered intrinsic, the donor-acceptor

strategy is prevalent, and many LSCs using donor-acceptor systems based on Förster resonance energy transfer (FRET) have been reported[20–24]. FRET permits efficient radiationless energy transfer between donors and acceptors, but only if the coupled molecules are within ≈ 5 nm of each other[9,17–19]. This degree of proximity in molecules containing large π-systems often leads to aggregation and decreased photoluminescence quantum efficiencies (PLQEs)[20–24], which hinder LSC performance. Combining the donor and acceptor species into one supramolecule can avoid this problem, albeit at the price of increased synthetic complexity[9,25]. One of the best examples of a donor-acceptor supramolecular system is the bacterial phycobilisome (Figure 1(c)). Phycobilisomes are highly organized complexes of different protein chromophores and linker peptides arranged to produce rapid and directional energy migration to a central core emitter[34]. Indeed phycobilisomes have been used directly in novel LSCs[16].

Boron-dipyrromethene (BODIPY) conjugated systems are a popular class of organic dyes that show high fluorescence yields and absorptivity, good photostability, and solubility in common solvents[35–38]. BODIPY dyes have been used as biological labels[39–41], laser dyes[42–44], monomer units in low-bandgap polymers[45–47], and in LSCs[15,48]. Due to aggregation, achieving efficient emission from a BODIPY dye in the solid state is difficult, but this can be remedied by incorporating the BODIPY core into a larger molecular scaffold[49–52]. In this work, we investigate LSCs containing a donor-acceptor system based on a central BODIPY emitter with three covalently-bound oligofluorene donor side units arranged in a star configuration (OFBMs, Figure 1 (b))[33]. The oligofluorene side units absorb light and transfer energy via FRET to the BODIPY core, where it is emitted. We study the effect of a systematic increase in the number of fluorene units per molecule.

The emission peak of the BODIPY core used in this work, at 610 nm (Figure 2 (a)), would not produce an effective LSC based on silicon PV cells. However, many proposed photo-bioreactors for the cultivation of microalgae are too expensive for practical applications due to the high cost of providing artificial illumination[53]. Further, it has been shown that spectral tuning can be used to improve growth efficiency for certain strains of microalgae and plants[54,55]. Thus LSCs based on OFBMs represent potentially useful candidates for lighting systems used in bioreactors[56]. Optimizing LSC efficiency is still important in this application. Through a concerted device and raytracing study, we find that interplay between the different effects of extending the oligofluorene donor arms mean simple heuristics for optimizing LSC efficiency are inadequate. Extending the OFBM structure through simulated spectra, we find

that this family of donor-acceptor molecules holds promise for low-reabsorption LSC applications.

Results

1. Steady-state optical properties of OFBMs

The OFBM molecules are named by the convention FnB, where *n* is the number of 9,9-dihexylfluorene units per arm. Molecules with *n* = 2, 3 and 4 were used (Figure 1 (b)), corresponding to 6, 9 and 12 fluorene units per BODIPY core. The OFBMs have a molar absorptivity of ≈ 80,000 $M^{-1}cm^{-1}$ in the BODIPY region and ≈ 30,000 $M^{-1}cm^{-1}$ per fluorene unit in the donor absorption region (Figure 2).

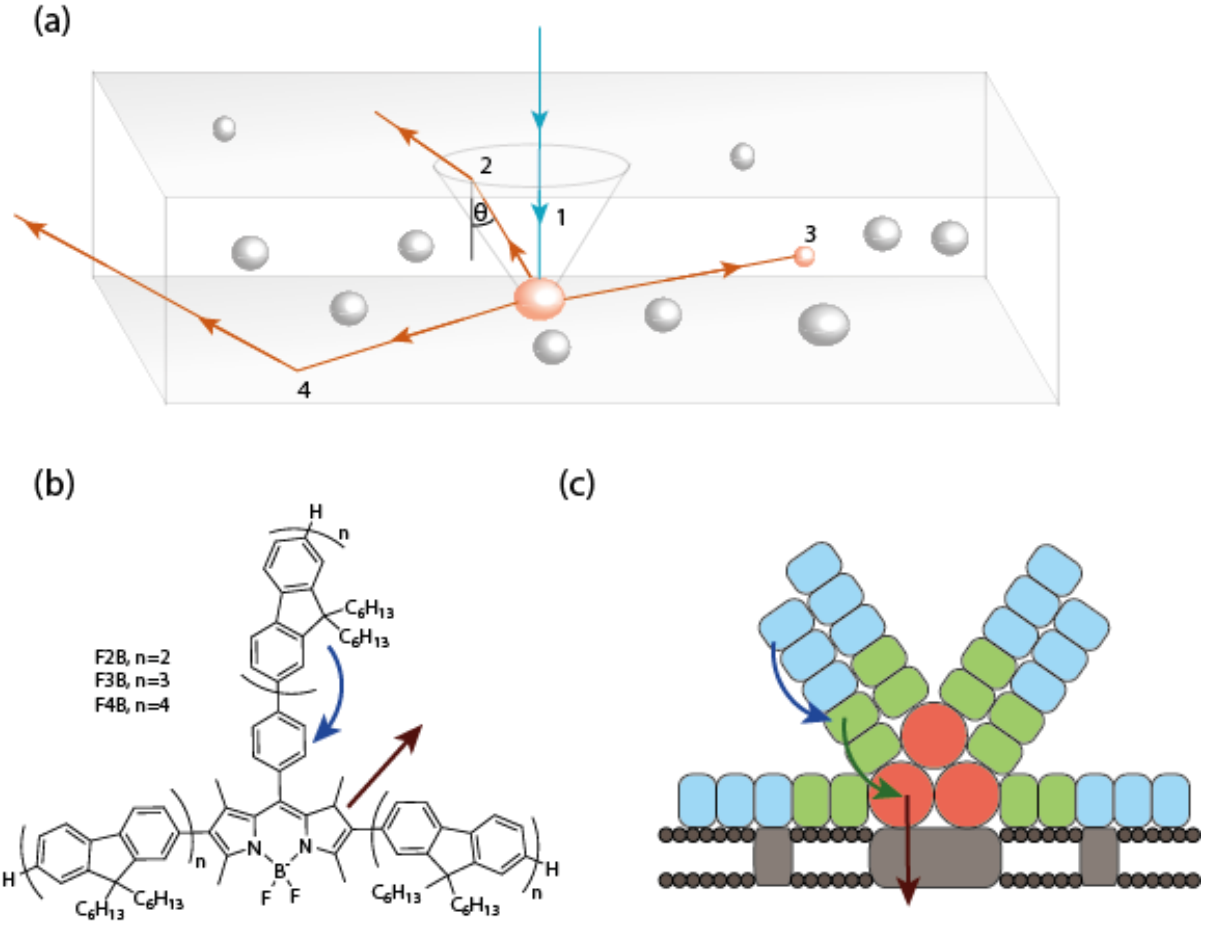

Figure 1: (a) Schematic representation of light trapping and total internal reflection in an LSC. The blue ray 1 represents the path of a solar photon absorbed by a dye molecule. The orange rays 2, 3 and 4 show three possible outcomes for a photon subsequently emitted. 2: The emitted photon enters an escape cone and is lost, which occurs if the angle of incidence upon the surface is less than the critical angle θ_c of the medium. 3: The photon is reabsorbed

by another identical dye molecule, re-priming the photon for loss through an escape cone or nonradiative decay. 4: The emitted photon propagates to an output aperture, where it can be usefully employed. Maximizing path 4 without sacrificing sunlight absorption is the key to designing efficient LSC devices. (b) The structures of the star-shaped oligofluorenes with BODIPY cores, FnB (n= 2-4). Arrows indicate energy transfer from the fluorene donors and emission from the BODIPY acceptor. (c) Structure of a phycobilisome with arrows showing transfer of excitons through the phycoerythrins (blue), phycocyanins (green) and allophycocyanis (red) to the thylakoid membrane (grey).

Moving from F2B through to F4B increases the intensity of the 350 nm absorption peak, due to the increased number of fluorene units, while the BODIPY peak intensity is unchanged. The position of the absorbance peak associated with the fluorene units undergoes a bathochromic shift of 13 nm per fluorene unit added to an arm (Supplementary Figure 1). This is due to extension of π conjugation through the oligofluorene arms[33].

Two-dimensional excitation-emission fluorescence spectra of the OFBMs (Figure 2 (b)-(d)) were collected at low optical density to minimize the inner filter effect. The spectra show that fluorescence occurs solely from the BODIPY core, much like in a phycobilisome. This suggests a high donor-acceptor energy transfer efficiency, which is in agreement with previous reports[33,57]. The increase in emission intensity for excitation at 360 nm compared to 540 nm correlates with the number of fluorene units. PLQEs were 0.70, 0.75 and 0.66 for F2B, F3B and F4B respectively, measured using a standard quinine disulfate reference[57].

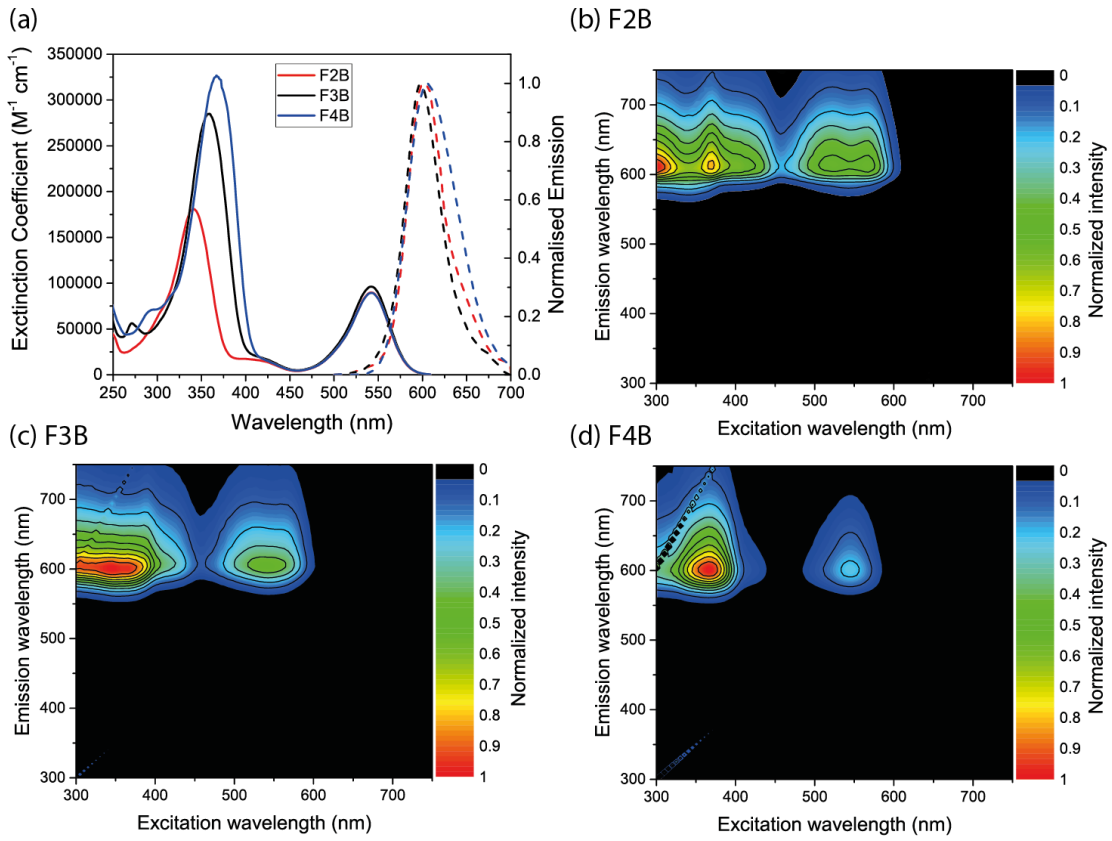

Figure 2: (a) Extinction and emission spectra of OFBMs in solution. (b)-(d) Two-dimensional emission/excitation spectra clearly showing that, under any excitation, emission occurs from the BODIPY core at 610 nm.

2. LSC fabrication

Three LSCs were fabricated using a polymer matrix of lauryl methacrylate (LMA):ethylene glycol dimethacrylate (EGDM) (4:1 by volume) doped with OFBM, prepared as described in the Methods section to give 10 cm × 10 cm × 0.3 cm waveguides. EGDM is a cross-linker that minimizes volume change during polymerisation, producing a rigid blend that is transparent in the visible[13,18,58–60]. The LSCs showed pronounced light emission from the narrow edges when excited with 365 nm and 532 nm illumination (Figure 3 (a) and Supplementary Figure 2). No changes in the dye absorption spectra were seen upon incorporation into the polymer matrix. Emission spectra showed a blue-shift relative to solution for all OFBMs (F2B ≈ 15 nm, F3B ≈ 10 nm, F4B ≈ 20 nm) (Figure 3 (b)-(d)). We attribute this to a change in the microenvironment of the BODIPY center, which is known to shift the emission spectrum[61]. The concentration of OFBM in the LSCs was 0.0130 mM,

0.0176 mM and 0.0126 mM for F2B, F3B and F4B respectively, as determined by absorption measurements.

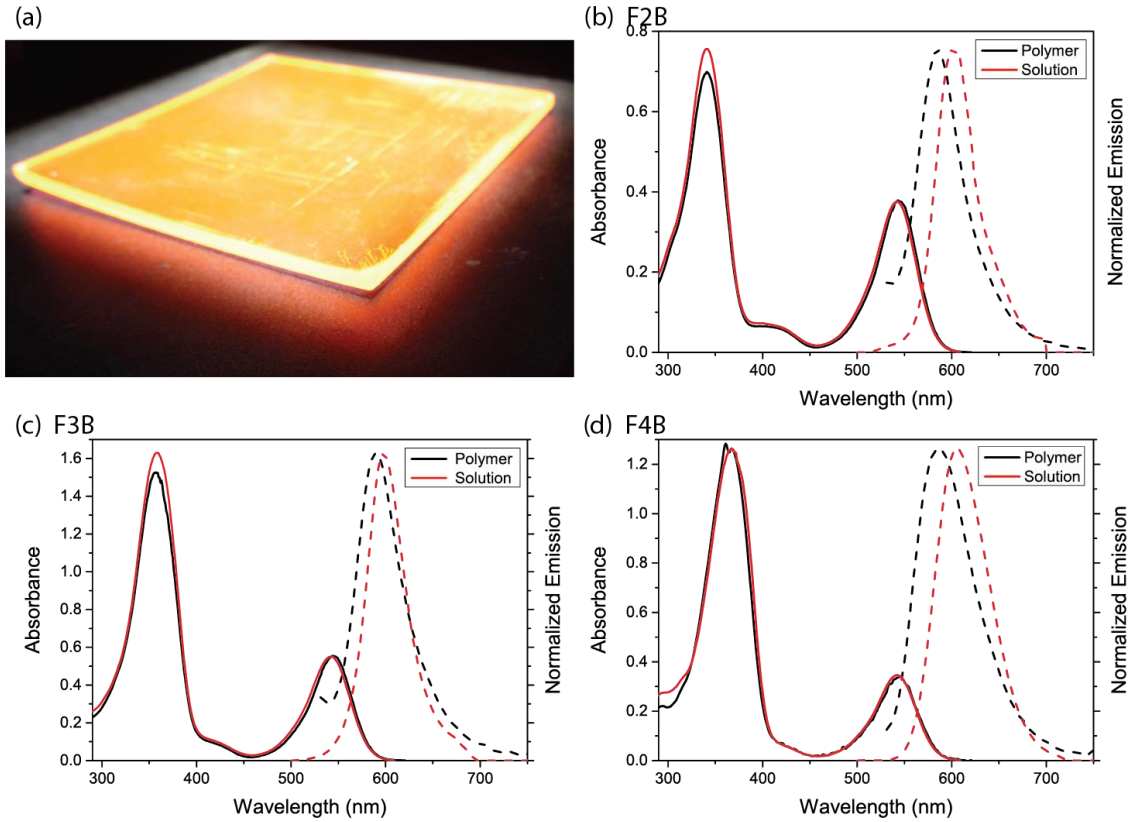

Figure 3: (a) LSC (F2B) photoexcited at 365 nm. Measured absorption and normalized emission of the LSCs (b) F2B, (c) F3B and (d) F4B.

3. LSC external quantum efficiency and flux gain

While the application of LSCs using the OFBM molecules studied is not anticipated to be in PV power generation, PV cells were used as convenient photodetectors in most of our device characterisations. Here, each LSC was coupled to four 10 x 0.3 cm silicon PV cells. No index matching between the LSC and PV cells was carried out. The current–voltage (I-V) characteristic of each LSC-PV system under AM 1.5G illumination was measured and used to calculate the external quantum efficiency (EQE), the ratio between the number of photons leaving the output aperture and the number of incident photons entering the input aperture. Using the measured absorption spectrum, we also calculated the internal quantum efficiency (IQE), the ratio of edge-emitted photons to photons absorbed by the LSC. EQEs and IQEs were simulated using the LSC raytrace program (see Methods section) with the experimental

parameters of concentration, absorbance and emission spectra, PLQY and device geometry as inputs. Measured and simulated EQEs and IQEs are shown in Table 1.

Using the simulation results, we calculated the flux gain, a detection-agnostic metric given by the ratio of photons leaving the output aperture to photons arriving over an equivalent area of the input aperture, for photons with energy exceeding a threshold value. For the three OFMBs measured, we chose a threshold of 700 nm, amenable to photobioreactors or some thin-film PV cells[53,62]. The flux gain at 700 nm (denoted F700) is shown in Table 1.

Table 1: Measured and simulated external and internal quantum efficiencies, and the calculated flux gain at 700 nm.

Sample	**Measured EQE (%)**	**Simulated EQE (%)**	**Measured IQE (%)**	**Simulated IQE (%)**	**F700**
F2B	1.69±0.15	1.71±0.02	36.4±3.3	37.6±0.3	0.47±0.02
F3B	2.44±0.33	2.73±0.03	38.2±5.2	42.8±0.2	0.76±0.04
F4B	1.82±0.17	1.91±0.02	34.7 ±3.2	36.5±0.4	0.53±0.04

The relatively narrow absorption bandwidth of the OFBMs means that much of the solar spectrum is not absorbed, thus it is unsurprising that the maximum measured EQE is only 2.44%, for F3B. F2B and F4B have EQEs of 1.69% and 1.82%, respectively. However, IQE values, which are not sensitive to incomplete absorption, are relatively high. F3B has an IQE of 38.4%, while F2B and F4B have IQEs of 36.4% and 34.7% respectively. There is good agreement between measurement and simulation results, which suggests raytracing can clarify the overlapping effects of changing PLQEs and emission spectrum blue-shifts among the three FnB materials. The calculated F700 values show a similar spread, peaking at 0.76 for F3B. We note that a sub-unity flux gain is unsurprising for the small size of the devices produced (G=8.3), and we show later that positive flux gain is predicted at a slightly larger G.

These results demonstrate that to understand the effect of oligofluorene length on LSC performance it is necessary to consider not just the influence of increasing donor relative to acceptor oscillator strength as the arms are lengthened, but also the effects of spectral shifts and changes in PLQE.

4. Spatially-dependent external quantum efficiency

Spatially-dependent EQE was measured by scanning a 2 × 2 mm square of AM 1.5G radiation across the surface of each LSC-PV device while measuring short-circuit photocurrent. 121 points were measured per device and then averaged over the four quadrants. EQE(x,y) was then calculated by dividing the total detected photocurrent, in units of *e*, by the incident photon flux. Simulations were conducted by spatially constraining the excitation source in the raytracer to mimic the grid of measurement points, and calculating EQE for each grid point. Measured and simulated results are presented in Figures 4 (a) and (b), respectively, and a one-dimensional comparison is shown in Figure 4 (c). A more detailed comparison between the measurements and simulations is presented in Supplementary Figure 3.

The low EQEs measured are again largely due to the high proportion of AM1.5G photons that are not absorbed by the OFBMs; our analysis therefore focuses on relative changes to the EQE with respect to excitation position, with the aim of clarifying the extent of reabsorption in these three devices. EQE(x,y) was found to decrease for all three devices as the excitation source was moved further from the edges, reflecting the greater likelihood of photon loss through reabsorption-driven nonradiative decay, outcoupling, and parasitic matrix processes as the average path length to reach the edge is increased. The simulation results agree reasonably well with the measurements, over-estimating the measured result by 5.2±1.5% at the outside corner positions. This difference is ascribed to an imperfect fabricated waveguide and PV cell optical coupling which is not accounted for in the simulations. The simulated and measured EQEs from the middle of the device differ by 9.2±0.7%, relative to each other; the additional difference seen here between experiment and simulation is accounted for by parasitic matrix losses which increase with path length and are not included in the simulations.

The relative drop in EQE for excitation in the middle of the LSC ($x = y = 5$ cm) compared to excitation directly adjacent to a corner is 32.1±3.4% for F2B, 24.2±2.0% for F3B and 24.2±1.6% for F4B. Although the F3B LSC has a higher OFBM concentration than the

others, this is counteracted by the slightly greater PLQE and smaller emission spectrum blue-shift of the molecule. The measured waveguide propagation losses are smaller than those reported for some simple nanocrystal devices, such as standard PbS (70% loss for a length of 8 cm[63]), and are approaching those of recently-reported core/shell $CuInSe_xS_{2-x}$/ZnS nanocrystals (30% loss at 12 cm[18]). Given the clear sensitivity of BODIPY core reabsorption loss to emission blue-shift and changes in PLQE, small improvements in both properties, which should be achievable by modifying the matrix material, will yield a very effective LSC emitter.

The degree of reabsorption associated with increased propagation length is determined by the spectral overlap between the luminophore emission and its absorbance spectrum. The spectrum of the emission from the output aperture was recorded as the propagation length increased. Excitation was by a 532 nm laser beam. All three LSCs showed a red shift in emission and a decrease in intensity with increasing distance (Figure 4 (d)) and Supplementary Figure 4 (a) (c) and (e)). These shifts stabilized at long path lengths as bluer photons were selectively eliminated by reabsorption. We simulated these results (Supplementary Figure 4(b) (d) and (f)), mimicking the narrow detection aperture and excitation source in the raytrace. The simulation results reproduce the experimental data to a large degree, showing the same trends in red-shift and intensity with increasing propagation length.

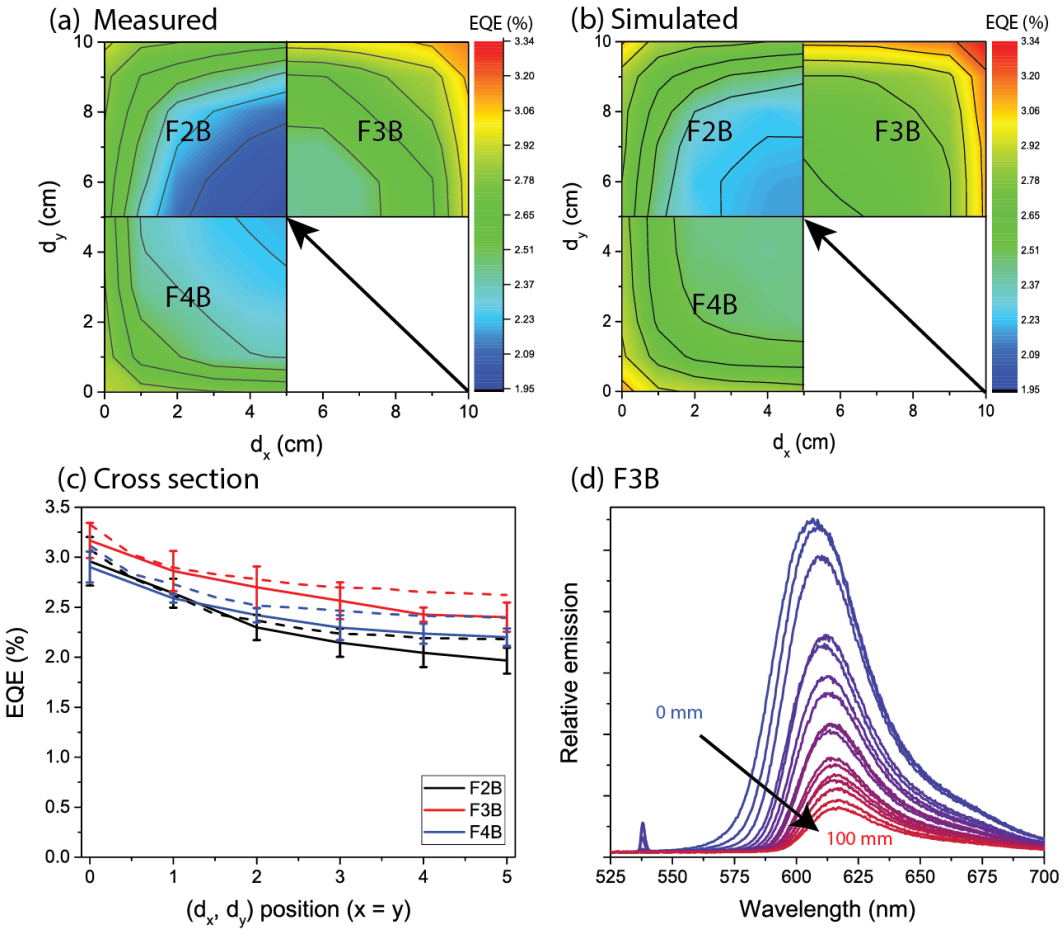

Figure 4: (a) Spatial maps of LSC EQE, reflecting the probability of incident sunlight generating emission from an LSC edge. Excitation was from a 2×2 mm square of AM 1.5G solar radiation. (b) Simulated results. Data represent counts collected from 10^6 incident photons. (c) EQE moving along a diagonal line drawn from the corner of the device to the center, for the measured data (solid line) and simulated data (dashed line). (d) Spectral changes in LSC edge emission spectra with excitation distance for the F3B LSC device. The peak at 532 nm is an artefact from the excitation spot

5. Spectrally-resolved external quantum efficiency

Spectrally-resolved EQE of the three LSCs was measured by affixing a small high-efficiency silicon PV cell to one edge of the LSC, and scanning the wavelength of a small monochromatic excitation spot held stationary near the attached cell. It is worth noting that the magnitude of the EQE is determined by the position of both the excitation spot and the PV cell. Simulations were conducted by constraining the excitation position and wavelength to match the experimental conditions. The measured and simulated EQEs are shown in Figure

5. The measurements are well-matched by the simulated results, when we allow for a non-zero baseline due to excitation source scatter and imperfect LSC-PV cell coupling.

The EQE in the ultraviolet increases as oligofluorene length increases, although the increase is not linear with fluorene count since the absorbed fraction scales logarithmically with optical density. The red-shifting of the oligofluorene feature accords with the measured absorption spectra. As expected, the EQE of the BODIPY feature is essentially constant across the three devices, with small differences ascribed to the PLQE and emission blue-shift differences of the three.

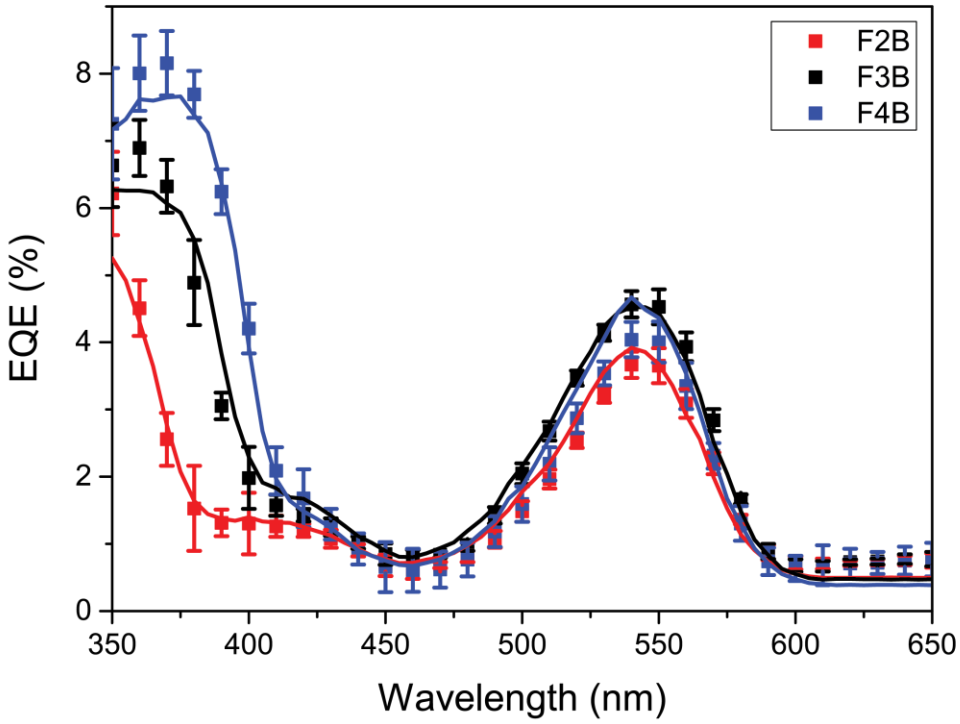

Figure 5: Spectrally-resolved external quantum efficiency of the fabricated LSC-PV system (squares) and simulated data (lines). Error bars represent the deviation in multiple EQE measurements.

6. Study of optimized devices using raytracing

As the simulation results accord with our experiments, we turn to simulations to predict the performance of optimized LSCs based on the three OFBMs studied. First, we repeated the EQE simulations presented in Table 1, maintaining the device geometry and PV cell characteristics, but stepping through dye concentration to find the optimum performance. The

results are shown in Figure 6 (a). A maximum EQE of 5.6% was found for F3B, roughly doubling the measured value, at a concentration of 0.25 mM. F2B and F4B both reached maximum EQEs of about 4.2% at similar concentrations. We note that the additional fluorene chromophores on F4B do not outweigh the penalties of increased emission blue-shift and decreased PLQE, and the EQE is on par with that of F2B for the device geometry studied.

Calculated F700 results are shown in Figure 6 (b). Much like the EQE results, F3B is the superior material, with flux gain approaching 1.0, while F2B and F4B show similar trends with concentration, peaking at 0.6. In our final simulation of these devices, we show that appreciable flux gains are possible: conducting a two-dimensional parameter sweep of geometric ratio and concentration (Figure 6 (c)-(e)), we find that the simulated flux gain of F3B exceeds 1.0 for a *G* of 9.9 (*G* of 14.7 for F2B and F4B), and plateaus at *F* = 7.1 at a *G* of 128 (*F* = 4.9 at a *G* of 138 for F2B and F4B). These flux gains are comparable to LSCs based on CdSe/CdS, $Cd_{0.999}Cu_{0.001}Se$ and Mn^{2+}-doped ZnSe/Zn core-shell quantum dots[13,62]. Large improvements to flux gain are anticipated if the absorption gap between the fluorene donor and the BODIPY core can be filled, which we approach in the next section.

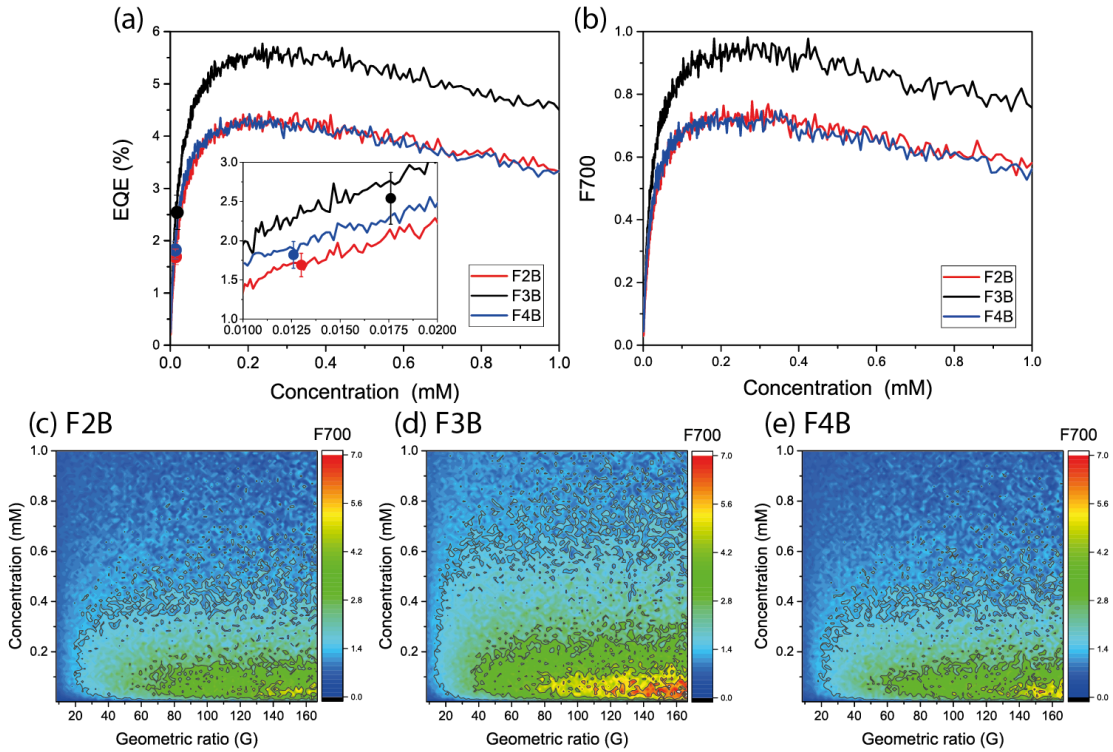

Figure 6: Results of Monte-Carlo ray trancing simulations of the three OFMBs studied. (a) EQEs using the same geometry and PV cell detectors utilized in actual measurements, as a function of dye concentration. Insert shows the low concentration region. Colored circles

represent our measurements of the fabricated LSCs. (b) Flux gain at 700nm as a function of concentration, for the same LSCs. Flux gain at 700 nm with changing concentration and geometric ratio for (c) F2B, (d) F3B and (e) F4B.

7. Simulations of extended dye structures

The potential applications of the LSCs studied above are inherently limited by solar flux in the UV region, low absorption coefficients in the visible region of the spectrum and an emission which is too high in energy. It is known that chromophores made from BODIPY cores and extended chromophore π-systems are highly versatile[64–66] and can be conveniently tailored to span the entire visible spectrum[67–69]. We present hypothetical structures that overcome these shortcomings by generating plausible absorption and emission spectra and testing their behavior in simulated LSCs. The BODIPY-fluorene systems presented in this study are synthesized without linker sections between the separate chromophores, allowing efficient energy transfer into the BODIPY core. We thus expect that this donor-acceptor scheme can be extended to larger structures with improved spectral coverage without significantly impairing energy transfer to the central emitter. Three hypothetical structures were studied: an OFBM containing 8 fluorenes per arm (F8B) (Figure 7 (a)); an OFBM with a new chromophore of intermediate energy inserted between the fluorene and the BODIPY (F8GB) (Figure 7 (c)); and two F8GB molecules connecting to a central deep-red emitter molecule (2(F8GB)D) (Figure 7 (e)). The hypothesized extinction and fluorescence spectra of these structures are shown in Figure 7(b),(d) and (f). The PLQE of the hypothetical molecules was set to 0.8, and all emission was assumed to occur from the core. Additional details on the likely reaction schemes that yield these structures are given in Supplementary Figure 5. We simulated EQE for each LSC using the same device geometry as the measured systems, and then simulated flux gain as a function of dye concentration and geometric ratio.

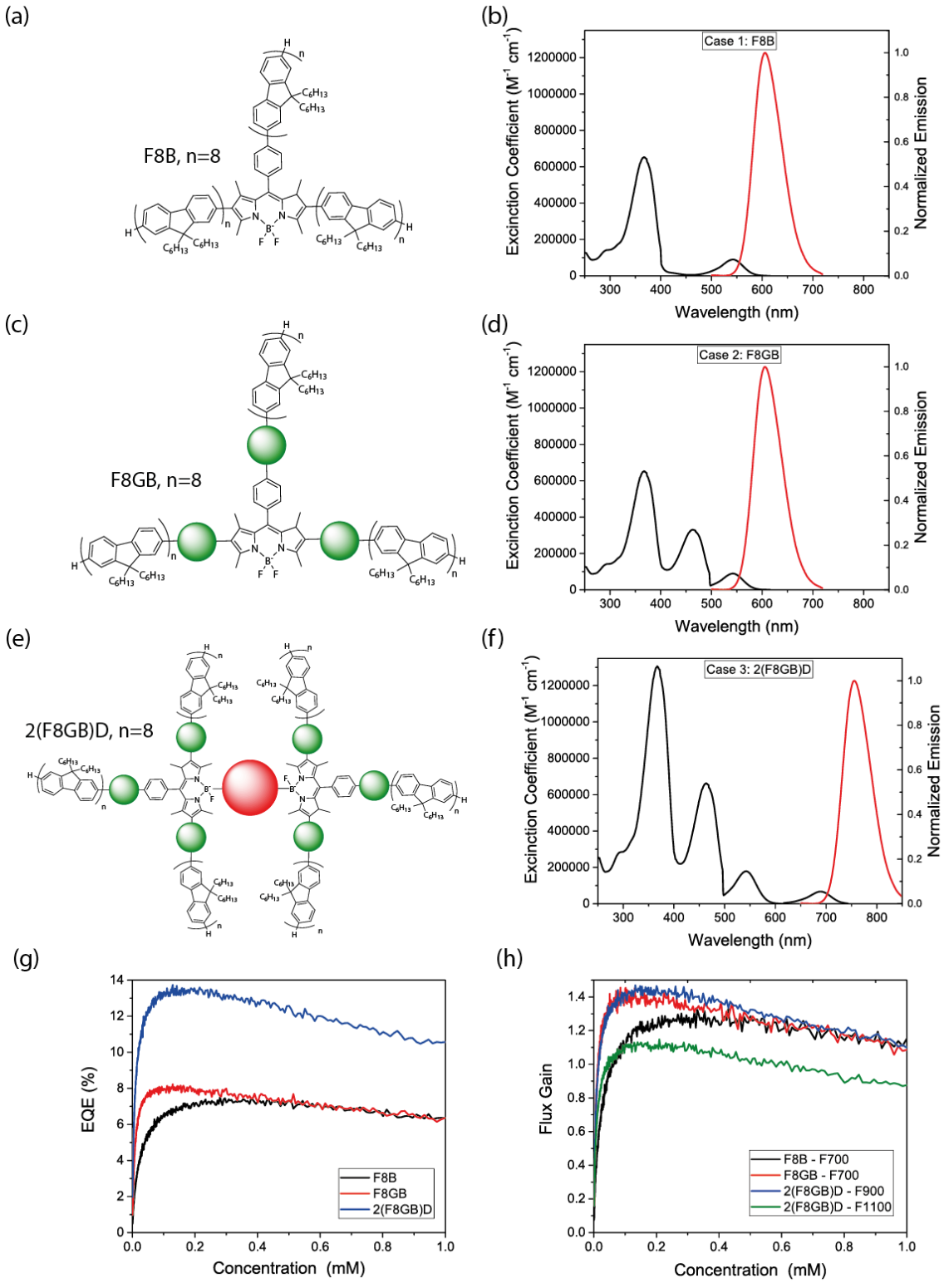

Figure 7. Molecular structures, steady-state optical spectra and results of Monte-Carlo ray trancing simulations of the hypothetical OFBMs. (a), (c) and (e) Molecular structure of F8B, F8GB and 2(F8GB)D, respectively. (d), (d) (f), Extinction and fluorescence spectra of the

respective materials. (g) EQE simulations for 10 x 10cm devices, (h) flux gain simulations for the same LSC geometry.

Simulated peak EQEs increased through the F8B, F8GB and 2(F8GB)D LSCs, and broadly followed the same trend with dye concentration (Figure 7 (g)). If these hypothetical molecules were used in our experimental set up they would produce peak EQEs of 7.2%, 8.0% and 13.4% respectively, which is a considerable gain over the molecules studied. This is due to the improved absorption of incident sunlight by the extended dye structures. Flux gains under specific thresholds for the 10 cm side-length devices (Figure 7 (h)) exceeded unity for all three materials, peaking at 1.30 and 1.43 for F8B and F8GB respectively at 700 nm, with concentration optimized. Considering that 2(F8GB)D has a redder emission than the other OFBMs studied, flux gains were calculated at 900 nm and 1100nm thresholds. Peak flux gains were found to be 1.45 and 1.13 respectively.

Two-dimensional flux gain simulations (Supplementary Figure 6) showed that F8B and F8GB reach F700 values of ≈ 10 and 16 at $G = 160$, while 2(F8GB)D has peak F900 and F1100 values of ≈ 15 and 12 respectively. While simulated flux gain continues to increase as we simulate yet-larger LSCs, in reality absorption in the matrix (an effect not included in the model) may start to dominate. For comparison, at G=160 recently synthesized $CuInS_2$/CdS core-shell quantum dots, which are reportedly the best-performing nanocrystalline emitters to date[62], show a projected flux gain of ~21 at the crystalline silicon band gap, while those of $Cd_{0.999}Cu_{0.001}Se$ and CdSe/CdS core-shell dots are projected to be ~7 and ~5, respectively[62]. These findings demonstrate that the potential of OFBMs and their analogues to achieve effective light concentration in LSCs is on a par with contemporary nanocrystalline materials. This warrants the synthesis and characterization of these larger donor-acceptor structures. With the addition of redder-emitting chromophores, OFBMs may even function effectively with silicon PV cells, assuming a moderately high PLQE can be maintained.

Conclusions

Oligofluorene-BODIPY donor-acceptor molecules represent attractive candidates for luminescent solar concentrators due to their synthetic versatility, high absorption coefficients, high PLQEs and efficient energy transfer to the BODIPY core. LSCs containing three

different OFBMs were fabricated and characterized using a variety of optical measurements. A Monte-Carlo raytracing simulation was used to successfully replicate these results. We subsequently used this simulation to study optimized LSCs based on the three starting compounds, along with three hypothetical OFBM structures which extended the donor-acceptor functionality in a plausible fashion. We found that in optimized conditions, the proposed OFBM molecules perform on-par with leading nanocrystalline emitters, warranting further investigation into the synthesis of these extended antennae complexes and their incorporation into LSCs.

Methods

Synthesis of oligofluorenes molecules: The oligofluorene molecules used in this study were synthesized with a modified Suzuki coupling using K_3PO_4[33]. Synthetic yields were between 29-58%. All molecules showed good thermal stability with decomposition temperatures above 400^{o}C.

Steady-state spectral measurements: Absorption spectra were measured using a HP 8453 spectrophotometer. Dye samples were dispersed in toluene at a concentration of ca. 1 mg ml^{-1} and a 1 mm path length was used. Film absorption spectra were measured using off-cuts from the produced LSCs. LSCs containing no active molecules were used as the blank. Photoluminescence measurements of solutions (1 mg ml^{-1} in toluene in a 1 mm cuvette) and films (thin off-cuts of the fabricated LSCs) including two-dimensional scans were measured on an Edinburgh Instruments FLS90 fluorimeter. The two-dimensional scans were normalized to the excitation intensity at each excitation wavelength

LSC fabrication: LSCs were formed by dissolving the chosen OFBM at ≈0.015 mM in an 4:1 solution of lauryl methacrylate (LMA) and ethylene glycol dimethacrylate (EGDM). The 4-methoxyphenol inhibitor, supplied with the monomers, was removed by passing the monomer solution over basic aluminum oxide. 2,2-Dimethoxy-2-phenyl acetophenone (1 wt.%) was added as an initiator and stirred until completely dissolved. The solution was placed in a mold made by two sheets of glass clamped together with a 0.3 cm thickness o-ring in-between. The o-ring in the mold sets the thickness of the LSCs to 0.3 cm. Polymerization occurred by exposure to 365 nm radiation for 5 hours. LSCs were cut and polished into 10 x 10 x 0.3 cm slabs.

LSC measurements: The LSCs were coupled to four 10 x 0.3 cm silicon PV cells (Sunpower, Slimfast C60E M 135, cut to size and connected in series, 0.55 % PCE) and current–voltage characteristics, and thus efficiency, were measured under AM 1.5G conditions using an Abet Sun 2000 solar simulator, at an intensity equivalent to 100 mW cm^2 after correcting for spectral mismatch, using a Keithley 2635 source measure unit. Current–voltage characteristics using a transparent LSC matrix without chromophores was also recorded to account for direct illumination of the PV cells by scattering of the excitation source; this contribution was subtracted.

LSC spatially-resolved EQE: For the spatial EQE measurements the LSC was illuminated by a 2×2 mm square of AM 1.5G solar radiation and overall current of the photodiodes was recorded at each (x,y) coordinate.

LSC edge emission: Spectral emission as a function of depth measurements was performed using a 523 nm laser pointer as the excitation source and edge emission was measured using a Labsphere CDS-610 spectrometer.

LSC spectrally-resolved EQE: A 100-W tungsten halogen lamp (400–1,500 nm) dispersed through a monochromator (Oriel Cornerstone 260) and a set of silicon diodes (ThorLabs SM05PD1A) was used for EQE measurements. A Keithley 2635 source measurement unit was used to measure the short-circuit current as a function of wavelength. The incident light was focused to a spot size of ca. 1 mm^2 using a set of lenses to illuminate the photodiode or LSC. For the LSC measurements the silicon photodiode (quantum efficiency 89.5% at the emission wavelength) was placed on the edge of the LSCs. The excitation position was in the center of the LSC, 5 mm from the edge.

Simulations: The LSC raytrace model was constructed in Matlab and has been previously reported.[70] LSC geometry was modelled as a square planar slab with a depth of 0.3 cm. The side length and dye concentration could be varied. In the simulation, unpolarized light, either drawn from the AM1.5G spectrum or at a specific wavelength, arrived on the upper face of the LSC at normal incidence. The absorption of sunlight and reabsorption of photoluminescence was determined probabilistically using the Beer–Lambert law. Wavelengths of incident and emitted photons were selected using the interpolation of a random unit scalar onto the relevant cumulative distribution function. Fresnel reflections and total internal reflection were simulated assuming a waveguide refractive index, n_r = 1.5, and air cladding (n_r = 1.0). The simulated LSCs had a uniform dye distribution throughout the

matrix, corresponding with the calculated concentration of the fabricated LSC devices. Each LSC was simulated with 10^6 incident photons; current was counted by logging photons traversing output apertures (the slab edges).

Acknowledgments:

N.J.L.K.D. is supported by the Cambridge Commonwealth European and International Trust, Cambridge Australian Scholarships and Mr Charles K Allen. R.W.M. acknowledges funding from the Initiative and Networking Fund of the Helmholtz Association. S.T. E. J. is supported by the Royal society. RGDT is supported by the EPSRC. D. C. thanks the Royal Society. PJS thanks the Royal Society for a Wolfson Research Merit Award. This work as supported by the EPSRC [EP/M005143/1, EP/M014797/1, EP/L012200/1]. We are grateful to Edward Booker for useful discussions. The authors acknowledge Professor Timothy Schmidt of the University of New South Wales for his input regarding the figures of merit used in this publication.

The data underlying this publication are available at https://doi.org/10.17863/CAM.7279.

Author contribution

N.J.L.K.D. carried out all experiments unless mentioned otherwise. R.W.M. wrote the simulation, helped N.J.L.K.D. with the simulations and performed the EQE simulation. S.T.E.J. Cut and polished the LSCs. C.O., D. C-L., R.G.D.T. and P.J.S. supplied the oligofluorenes. N.J.L.K.D., R.W.M., D.C. and N.C.G. contributed to writing the manuscript, and all authors contributed to discussion and analysis of the results.

References:

(1) Debije, M. G.; Verbunt, P. P. C. *Adv. Energy Mater.* **2012**, *2*, 12–35.

(2) Batchelder, J. S.; Zewail, A. H.; Cole, T. *Appl. Opt.* **1979**, *18*, 3090–3110.

(3) van Sark, W. G. J. H. M. *Renew. Energ.* **2012**, 1–4.

(4) van Sark, W. G. J. H. M.; Barnham, K. W. J.; Slooff, L. H.; Chatten, A. J.; Buechtemann, A.; Meyer, A.; McCormack, S. J.; Koole, R.; Farrell, D. J.; Bose, R.; Bende, E. E.; Burgers, A. R.; Budel, T.; Quilitz, J.; Kennedy, M.; Meyer, T.; De, M. D. C.; Meijerink, A.; Vanmaekelbergh, D. *Opt. Express* **2008**, *16*, 21773–21792.

(5) Delavari Amrei, H.; Ranjbar, R.; Rastegar, S.; Nasernejad, B.; Nejadebrahim, A. *J. Appl. Phycol.* **2014**, 67–74.

(6) Earp, A. A.; Smith, G. B.; Franklin, J.; Swift, P. *Sol. Energy Mater. Sol. Cells* **2004**, *84*, 411–426.

(7) Manousiadis, P. P.; Rajbhandari, S.; Mulyawan, R.; Vithanage, D. A.; Chun, H.; Faulkner, G.; O'Brien, D. C.; Turnbull, G. A.; Collins, S.; Samuel, I. D. W. *Optica* **2016**, *3*, 702–706.

(8) Giebink, N. C.; Wiederrecht, G. P.; Wasielewski, M. R. *Nat. Photonics* **2011**, *5*, 694–701.

(9) Farrell, D.; Yoshida, M. *Prog. Photovoltaics Res. Appl.* **2012**, *20*, 93–99.

(10) Roncali, J.; Garnier, F. *Appl. Opt.* **1984**, *23*, 2809–2817.

(11) Olson, R. W.; Loring, R. F.; Fayer, M. D. *Appl. Opt.* **1981**, *20*, 2934–2940.

(12) Wilson, L. R.; Rowan, B. C.; Robertson, N.; Moudam, O.; Jones, A. C.; Richards, B. S. *Appl. Opt.* **2010**, *49*, 1651–1661.

(13) Erickson, C.; Bradshaw, L. *ACS Nano* **2014**, 3461–3467.

(14) Wilson, L. R.; Richards, B. S. *Appl. Opt.* **2009**, *48*, 212–220.

(15) Bailey, S. T.; Lokey, G. E.; Hanes, M. S.; Shearer, J. D. M.; McLafferty, J. B.; Beaumont, G. T.; Baseler, T. T.; Layhue, J. M.; Broussard, D. R.; Zhang, Y.-Z.; Wittmershaus, B. P. *Sol. Energy Mater. Sol. Cells* **2007**, *91*, 67–75.

(16) Mulder, C. L.; Theogarajan, L.; Currie, M.; Mapel, J. K.; Baldo, M. A.; Vaughn, M.; Willard, P.; Bruce, B. D.; Moss, M. W.; McLain, C. E.; Morseman, J. P. *Adv. Mater.* **2009**, *21*, 3181–3185.

(17) Davis, N. J. L. K.; MacQueen, R. W.; Roberts, D. A.; Danos, A.; Dehn, S.; Perrier, S.; Schmidt, T. W. *J. Mater. Chem. C* **2016**, *4*, 8270–8275.

(18) Meinardi, F.; McDaniel, H.; Carulli, F.; Colombo, A.; Velizhanin, K. A.; Makarov, N. S.; Simonutti, R.; Klimov, V. I.; Brovelli, S. *Nat. Nanotechnol.* **2015**, *10*, 878–885.

(19) Meinardi, F.; Colombo, A.; Velizhanin, K. A.; Simonutti, R.; Lorenzon, M.; Beverina, L.; Viswanatha, R.; Klimov, V. I.; Brovelli, S. *Nat. Photonics* **2014**, *8*, 392–399.

(20) Balaban, B.; Doshay, S.; Osborn, M.; Rodriguez, Y.; Carter, S. A. *J. Lumin.* **2014**, *146*, 256–262.

(21) Tummeltshammer, C.; Taylor, A.; Kenyon, A. J.; Papakonstantinou, I. *J. Appl. Phys.* **2014**, *116*.

(22) Banal, J. L.; Ghiggino, K. P.; Wong, W. W. H. *Phys. Chem. Chem. Phys.* **2014**, *16*, 25358–25363.

(23) Banal, J. L.; Soleimaninejad, H.; Jradi, F. M.; Liu, M.; White, J. M.; Blakers, A. W.; Cooper, M. W.; Jones, D. J.; Ghiggino, K. P.; Marder, S. R.; Smith, T. A.; Wong, W. W. H. *J. Phys. Chem. C* **2016**, *120*, 12952–12958.

(24) Kaniyoor, A.; Mckenna, B.; Comby, S.; Evans, R. C. *Adv. Opt. Mater.* **2016**, *4*, 444–456.

(25) Förster, T. *Discuss. Faraday Soc.* **1959**, *27*, 7–17.

(26) Roberts, D. V; Wittmershaus, B. P.; Zhang, Y.-Z.; Swan, S.; Klinosky, M. P. *J. Lumin.* **1998**, *79*, 225–231.

(27) Fennel, F.; Lochbrunner, S. *Phys. Chem. Chem. Phys.* **2011**, *13*, 3527–3533.

(28) Calzaferri, G.; Meallet-Renault, R.; Bruhwiler, D.; Pansu, R.; Dolamic, I.; Dienel, T.; Adler, P.; Li, H.; Kunzmann, A. *Chem. Phys. Chem* **2011**, *12*, 580–594.

(29) Braslavsky, S. E.; Fron, E.; Rodríguez, H. B.; Román, E. S.; Scholes, G. D.; Schweitzer, G.; Valeur, B.; Wirz, J. *Photochem. Photobiol. Sci.* **2008**, *7*, 1444–1448.

(30) Bruehwiler, D.; Calzaferri, G.; Torres, T.; Ramm, J. H.; Gartmann, N.; Dieu, L.-Q.; Lopez-Duarte, I.; Martinez-Diaz, M. V. *J. Mater. Chem.* **2009**, *19*, 8040–8067.

(31) Eisfeld, A.; Briggs, J. S. *Chem. Phys.* **2006**, *324*, 376–384.

(32) Neuteboom, E. E.; Meskers, S. C. J.; Meijer, E. W.; Janssen, R. A. J. *Macromol. Chem. Phys.* **2004**, *205*, 217–222.

(33) Orofino-Pena, C.; Cortizo-Lacalle, D.; Cameron, J.; Sajjad, M. T.; Manousiadis, P. P.; Findlay, N. J.; Kanibolotsky, A. L.; Amarasinghe, D.; Skabara, P. J.; Tuttle, T.; Turnbull, G. A.; Samuel, I. D. W. *Beilstein J. Org. Chem.* **2014**, *10*, 2704–2714.

(34) MacColl, R. *J. Struct. Biol.* **1998**, *124*, 311–334.

(35) Loudet, A.; Burgess, K. *Chem. Rev.* **2007**, *107*, 4891–4932.

(36) Ziessel, R.; Ulrich, G.; Harriman, A. *New J. Chem.* **2007**, *31*, 496–501.

(37) Ulrich, G.; Ziessel, R.; Harriman, A. *Angew. Chemie - Int. Ed.* **2008**, *47*, 1184–1201.

(38) Benniston, A. C.; Copley, G. *Phys. Chem. Chem. Phys.* **2009**, *11*, 4124–4131.

(39) Courtis, A. M.; Santos, Sofia, A.; Guan, Y.; Hendricks, J. A.; Ghosh, B.; Szantai-kis, D. M.; Reis, S. A.; Shah, J. V; Mazitschek, R. *Bioconjug. Chem.* **2014**, *25*, 1043–1051.

(40) Moriarty, R. D.; Martin, A.; Adamson, K.; O'Reilly, E.; Mollard, P.; Forster, R. J.; Keyes, T. E. *J. Microsc.* **2014**, *253*, 204–218.

(41) Ni, Y.; Wu, J. *Org. Biomol. Chem.* **2014**, *12*, 3774–3791.

(42) Duran-Sampedro, G.; Agarrabeitia, A. R.; Garcia-Moreno, I.; Costela, A.; Banuelos, J.; Arbeloa, T.; Lopez Arbeloa, I.; Chiara, J. L.; Ortiz, M. J. *European J. Org. Chem.* **2012**, 6335–6350.

(43) Bañuelos, J.; Martín, V.; Gómez-Durán, C. F. A.; Córdoba, I. J. A.; Peña-Cabrera, E.; García-Moreno, I.; Costela, Á.; Pérez-Ojeda, M. E.; Arbeloa, T.; Arbeloa, Í. L. *Chem. - A Eur. J.* **2011**, *17*, 7261–7270.

(44) Ortiz, M. J.; Garcia-Moreno, I.; Agarrabeitia, A. R.; Duran-Sampedro, G.; Costela, A.; Sastre, R.; Lopez Arbeloa, F.; Banuelos Prieto, J.; Lopez Arbeloa, I. *Phys. Chem. Chem. Phys.* **2010**, *12*, 7804–7811.

(45) Cortizo-Lacalle, D.; Howells, C. T.; Gambino, S.; Vilela, F.; Vobecka, Z.; Findlay, N. J.; Inigo, A. R.; Thomson, S. a. J.; Skabara, P. J.; Samuel, I. D. W. *J. Mater. Chem.* **2012**, *22*, 14119.

(46) Popere, B. C.; Della Pelle, A. M.; Poe, A.; Balaji, G.; Thayumanavan, S. *Chem. Sci.* **2012**, *3*, 3093.

(47) Popere, B. C.; Della Pelle, A. M.; Thayumanavan, S. *Macromolecules* **2011**, *44*, 4767–4776.

(48) Altan Bozdemir, O.; Erbas-Cakmak, S.; Ekiz, O. O.; Dana, A.; Akkaya, E. U. *Angew. Chemie - Int. Ed.* **2011**, *50*, 10907–10912.

(49) Kanibolotsky, A. L.; Perepichka, I. F.; Skabara, P. J. *Chem. Soc. Rev.* **2010**, *39*, 2695–2728.

(50) Adronov, A.; Fréchet, J. M. J. *Chem. Commun.* **2000**, 1701–1710.

(51) Guliyev, R.; Coskun, A.; Akkaya, E. U. *J. Am. Chem. Soc.* **2009**, *131*, 9007–9013.

(52) Yilmaz, M. D.; Bozdemir, O. A.; Akkaya, E. U. *Org. Lett.* **2006**, *8*, 2871–2873.

(53) Chen, C. Y.; Yeh, K. L.; Aisyah, R.; Lee, D. J.; Chang, J. S. *Bioresour. Technol.* **2011**,

102, 71–81.

(54) Mohsenpour, S. F.; Richards, B.; Willoughby, N. *Bioresour. Technol.* **2012**, *125*, 75–81.

(55) Johkan, M.; Shoji, K.; Goto, F.; Hahida, S.; Yoshihara, T. *Environ. Exp. Bot.* **2012**, *75*, 128–133.

(56) Mohsenpour, S. F.; Willoughby, N. *Bioresour. Technol.* **2013**, *142*, 147–153.

(57) Sajjad, M. T.; Manousiadis, P. P.; Orofino, C.; Cortizo-Lacalle, D.; Kanibolotsky, A. L.; Rajbhandari, S.; Amarasinghe, D.; Chun, H.; Faulkner, G.; O'Brien, D. C.; Skabara, P. J.; Turnbull, G. A.; Samuel, I. D. W. *Adv. Opt. Mater.* **2015**, *3*, 536–540.

(58) Bomm, J.; Büchtemann, A.; Chatten, A. J.; Bose, R.; Farrell, D. J.; Chan, N. L. A.; Xiao, Y.; Slooff, L. H.; Meyer, T.; Meyer, A.; van Sark, W. G. J. H. M.; Koole, R. *Sol. Energy Mater. Sol. Cells* **2011**, *95*, 2087–2094.

(59) Bomm, J.; Büchtemann, A.; Fiore, A.; Manna, L.; Nelson, J. H.; Hill, D.; van Sark, W. G. J. H. M. *Beilstein J. Nanotechnol.* **2010**, *1*, 94–100.

(60) Bronstein, N.; Li, L.; Xu, L.; Yao, Y. *ACS Nano* **2014**, *8*, 44–53.

(61) Yang, X.; Zhang, X. F.; Lu, X.; Yu, C.; Jiao, L. *J. Photochem. Photobiol. A Chem.* **2015**, *297*, 39–44.

(62) Knowles, K. E.; Kilburn, T. B.; Alzate, D. G.; McDowall, S.; Gamelin, D. R. *Chem. Commun.* **2015**, *51*, 9129–9132.

(63) Shcherbatyuk, G. V.; Inman, R. H.; Wang, C.; Winston, R.; Ghosh, S. *Appl. Phys. Lett.* **2010**, *96*, 191901.

(64) Li, L.; Han, J.; Nguyen, B.; Burgess, K.; Li, L.; Han, J.; Nguyen, B.; Burgess, K. *J. Org. Chem.* **2008**, *73*, 1963–1970.

(65) Ozdemir, T.; Atilgan, S.; Kutuk, I.; Yildirim, L. T.; Tulek, A.; Bayindir, M.; Akkaya, E. U. *Org. Lett.* **2009**, *11*, 2105–2107.

(66) Erbas, S.; Gorgulu, A.; Kocakusakogullari, M.; Akkaya, E. U. *Chem. Commun.* **2009**, 4956–4958.

(67) Wang, D.; Fan, J.; Gao, X.; Wang, B.; Sun, S.; Peng, X. *J. Org. Chem.* **2009**, *74*, 7675–7683.

(68) Rurack, K.; Kollmannsberger, M.; Daub, J. *Angew. Chemie - Int. Ed.* **2001**, *40*, 385–

387.

(69) Umezawa, K.; Nakamura, Y.; Makino, H.; Citterio, D.; Suzuki, K. *J. Am. Chem. Soc.* **2008**, *130*, 1550–1551.

(70) MacQueen, R. W.; Tayebjee, M. J. Y.; Webb, J. E. A.; Falber, A.; Thordarson, P.; Schmidt, T. W. *J. Opt.* **2016**, *18*, 064010.

Table of Contents Figure and Text

Energy transfer in star-shaped donor-acceptor molecules reduces self-absorption in luminescent solar concentrators.